Research Article

Daniel Flamm*, Julian Hellstern, Myriam Kaiser, Max Kahmann, Jonas Kleiner, and Christoph Tillkorn

Light along curves: Photonic shaping tools

https://doi.org/10.3389/aot.2023.1237132
Received June 08, 2023; revised June 13, 2023; accepted July 26, 2023

Abstract: A structured light concept is reported enabling to distribute a large number of focus copies at arbitrary positions in a working volume. Applying this holographic 3D-beam splitter concept to ultrashort laser pulses allows to deposit energy along accelerating trajectories in the volume of transparent materials. Based on the entirety of the volume modifications created in this way, the material can be separated, for example, to create chamfered glass edges. These photonic tools impress with enormous versatility, which enable equally diverse application strategies ranging from cutting and welding to data storing.

Keywords: Ultrafast optics, Glass processing, Structured light, Micro-machining

Preprint of the original article:
D. Flamm, J. Hellstern, M. Kaiser, M. Kahmann, J. Kleiner, and C. Tillkorn, "Light along curves: Photonic shaping tools," Advanced Optical Technologies, **12**, 1237132, 2023.
https://doi.org/10.3389/aot.2023.1237132

1 Introduction

Since the theoretical description [1] and experimental realization [2] of the optical Airy beam by Siviloglou *et al.*, accelerating beams have caused a stir in the scientific world as they appear to violate the fundamental property of straight light propagation [3]. Since then, a large number of applications have been proposed and realized [3] including ultrafast micromachining along curves already demonstrated in 2012 by Mathis *et al.* [4]. The self-healing properties of this class of radiation are shown to be particularly useful, as local material modifications usually prevent undisturbed light propagation. To the same extent as known from non-diffracting beams [5], Airy beam profiles reconstitute themselves behind obstacles including highest peak intensities, enabling particularly efficient processing of substrates in a single pass [4]. Therefore, this class of radiation is also called non-diffracting second type [6, 7].

The Airy beam and related caustic-based concepts [3, 8] certainly owe their academic triumph (the keyword "Airy beam" yields several thousand papers at google scholar) to the general accessibility of liquid-crystal-on-silicon-based spatial light modulators (SLMs). In most cases, matched phase masks, for example cubic phase modulations (far-field generation) [2] or the well-known "3/2-phase pattern" (near-field generation) [9], displayed by SLMs and embedded in simple focusing [2] or imaging [8] optics form the optical setup. As the spatial resolution of today's SLMs allows only a few degree in diffraction angles, the degree of curvature is mainly determined by the numerical aperture (NA) of the focusing used. If, for example, maximum angle differences of the tangents to the curved surface of 90-deg are to be aimed, the required

***Corresponding author: Daniel Flamm,** TRUMPF Laser- und Systemtechnik GmbH, Johann-Maus-Str. 2, 71254 Ditzingen, Germany, e-mail: daniel.flamm@trumpf.com
Julian Hellstern, Christoph Tillkorn, TRUMPF Laser GmbH, Aichhalder Str. 39, 78713 Schramberg, Germany
Myriam Kaiser, Max Kahmann, Jonas Kleiner, TRUMPF Laser- und Systemtechnik GmbH, Johann-Maus-Str. 2, 71254 Ditzingen, Germany,

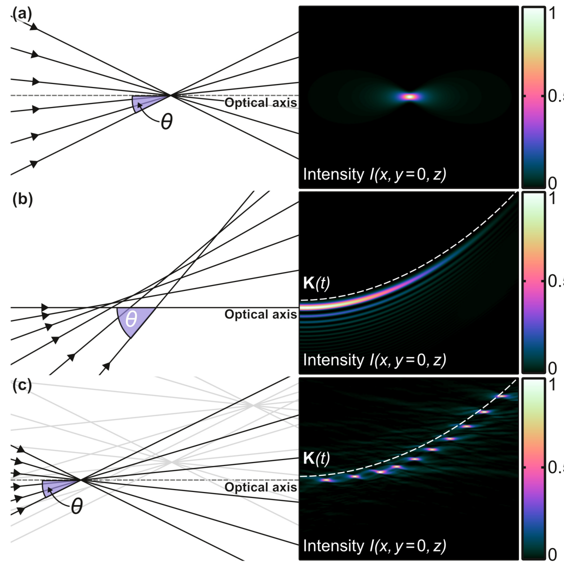

Fig. 1: Ray optical and wave optical representation of different focus distributions propagating in vacuum without applying an optical potential. As for the wave optical case, normalized intensity cross sections $I\left(x, y=0, z\right)$ are shown. Clear length or intensity units are not labeled by intention, since a qualitative discussion is sufficient here. Gaussian focus (a), Airy focus distribution (b) [8], and 3D-focus distribution (c) [14] sampling a similar accelerating trajectory $\mathbf{K}\left(t\right)=\left(x\left(t\right), y\left(t\right), z\left(t\right)\right)$. In all cases laser light propagates from left to right, parallel to the optical axis, illuminates a beam shaping element and is focused. The required numerical aperture (NA) is indicated by maximal half-angle θ of the cone of light that can enter or exit the lens (beam shaping element and focusing lens not shown). In this and in some of the following figures we make use of Green's colorscheme [15].

NA is already 1, cf. Fig. 1. Such "strong" focusings to generate nonparaxial accelerating beams [8, 10] can of course be realized by conventional microscope objectives, see for example the NA-0.8-micromachining experiment in Ref. [4]. For industry-grade materials processing, however, this entails various disadvantages, e.g. with respect to working distance, focus position tolerance, or lens contamination or collisions. To name just one example: Considering a microscope objective with NA = 0.8, the resulting working distance is typically well below 1 mm. The risk of constant lens contamination by micro-debris during materials processing is very high.

Recently, several studies have been published in which glass edges formed with accelerating and tilted non-diffracting beams have been fabricated in a single pass, see Refs. [11–13]. The edge shapes produced and in particular the only slightly reduced edge angles support our argument that a more advanced tool is needed enabling trajectories with 45-deg tangential angles to the surface.

Our solution for a photonic shaping tool, i.e., the generation of high intensities along arbitrary curves or surfaces to modify materials, is based on distributing a large number of focus copies in the processing volume. Here, the desired spatial shape is sampled by discrete foci whose entirety form the total focus distribution, see Fig. 1 (c). We will demonstrate that almost arbitrary tangential angles to the accelerated trajectory are possible, as well as the sampling of arbitrarily curved surfaces. The requirements on the numerical aperture of the focusing objectives are moderate, so that large working distances and large working volumes are possible at the same time. The ability to process large working volumes simultaneously allows to fully exploit the power or energy performance of industrial laser systems and to develop particularly efficient laser application strategies. In the paper, the two main enabler of this concept, the central beam splitting element, here, again realized with, for example, flexible SLMs, cf. Sec. 2, and the advanced focusing unit, cf. Sec. 3, are introduced in detail.

We have identified the processing of transparent materials as a main application of this concept. Here, we can use the high intensities generated by ultrashort laser pulses, to deterministically deposit energy in the volume of glasses with light. At the resulting modified areas, the material can be separated, e.g., by applying a selective etching strategy. In Sec. 4, we will apply our shaping tools to cut display glasses with tailored edges in a single pass. The substrates with laser-chamfered edges show enhanced mechanical properties when it comes to an impact or when the sample already exhibits smallest defects from former fabrication steps [16]. Here, the photonic shaping tool has the potential to replace conventional techniques based on mechanical grinding and polishing [17].

2 Holographic 3D-beam splitter

Industrial ultrafast laser sources providing multi-kilowatts of average powers and several tens-of-millijoules pulse energies will be available soon [18–21]. These laser systems enable the development of completely new application strategies, such as, e.g. single-pass, millimeter-scaled cutting of glasses with m/s-feed rates [22, 23]. This simple example illustrates the need for sophisticated optical concepts, since the simultaneous processing of the entire substrate thickness using an adapted non-diffracting beam [23], is the key to make efficient use of the extreme laser parameters. Therefore, processing optics are of particular interest that distribute high laser intensities into large volumes, cf. glass cutting example [23, 24], or onto large surfaces [25, 26] in order to increase throughput through parallel processing and, thus, to exploit the full performance of the laser source [27]. Based on well-known techniques for parallel data recording and storing [28–31], here, we use concepts to generate multifocal arrays and extend them to arbitrarily place a multitude of foci within a millimeter-scaled working volume [32, 33].

Displacing a focal spot from its original geometric focus position behind a lens is achieved by introducing phase modifications to the illuminating optical field. In terms of Zernike polynomials [34], a proper choice of tip/tilt modes in combination with a defocus allows to control the transverse $(\Delta x, \Delta y)$ and longitudinal Δz displacement, respectively. This simple approach for the manipulation of a single focus is extended to a 3D-beam splitting concept by exploiting the linearity property of optics and multiplex the corresponding holographic transmission functions—one for each focus to be placed in the working volume [35, 36].

Transverse shifting the jth-order focus is achieved by setting a linear blaze grating $T_j^{\text{blaze}}(\mathbf{r})$ with spatial frequency $\mathbf{K}_j = (K_{x,j}, K_{x,j})$ in the front focal plane of a lens with focal length f_{FL}. The corresponding transmission function then reads as [37]

$$T_j^{\text{blaze}}(\mathbf{r}) = \exp\left[\imath\left(\mathbf{K}_j\mathbf{r} + \phi_j\right)\right] \tag{1}$$

and yields a transverse displacement according to $\Delta x_j = f_{\text{FL}} \tan\left[\sin^{-1}\left(\lambda K_{x,j}/2\pi\right)\right]$, deduced from the grating equation (straightforward for the displacement in y-direction). We additionally define the constant phase offset ϕ_j to manipulate the absolute phase values of respective diffraction order j, which we will need later for the realization of 3D-beam splitter as a pure phase hologram [36].

Longitudinal displacement Δz_j of the focal spot of order j is realized by introducing the defocus mode [34] using, e.g., a holographic lens transmission with focal length f_j [38]

$$T_j^{\text{lens}}(\mathbf{r}) = \exp\left[\imath\pi r^2/\left(\lambda f_j\right)\right]. \tag{2}$$

In paraxial approximation the longitudinal shift is directly deduced from $\Delta z_j \approx -f_{\text{FL}}^2/\left(f_{\text{FL}} + f_j\right)$. Please note that instead of ideal lens transmissions T_j^{lens}, spot-dependent phase corrections could be applied additionally. For example, to compensate for spherical aberrations, caused by real focusing units, cf. Sec. 3, or when spots are focused deep behind an optical interface [39].

Combinations of transverse $(\Delta x_j, \Delta y_j)$ and longitudinal (Δz_j) shifts are achieved by multiplying both transmissions $T_j = T_j^{\text{blaze}} T_j^{\text{lens}}$. Multiplexing these $j_{\max}$ transmission functions will yield the total transmission which reads as [36]

$$T^{\text{tot}}(\mathbf{r}) = \sum_j^{j_{\max}} T_j = \sum_j^{j_{\max}} T_j^{\text{blaze}}(\mathbf{r})\, T_j^{\text{lens}}(\mathbf{r}). \tag{3}$$

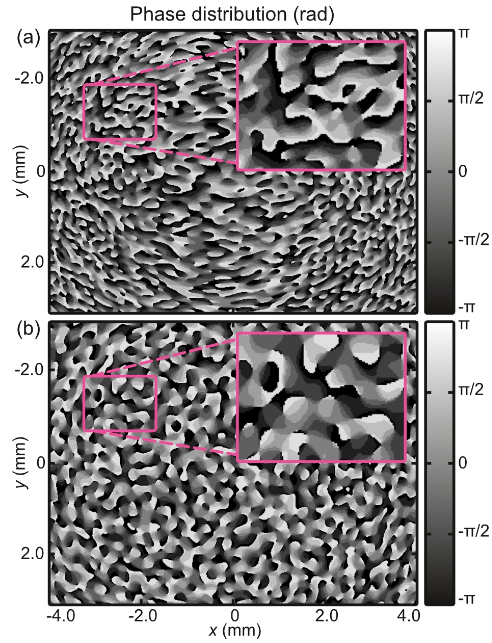

Fig. 2: Central details of phase modulations defining the phase-only transmission functions $T^{\mathrm{tot}}(\mathbf{r})$. The example depicted in (a) generates the spiral-like focus trajectory shown in Fig. 3. The second subfigure (b) represents the beam splitting element to distribute focus copies along the cone surface presented in Fig. 3. Both elements were optimized to be realized as quantized 8-level elements, see insets, fabricated via laser lithography in fused silica [16]. These distributions are reminiscent of those used for 2D diffractive beamsplitters [44], but the periodic sequel of unit cells is absent due to the holographic lenses, cf. Eq. (2). In contrast to classical 2D beam splitters, 3D beam splitter elements must therefore be spatially aligned to the raw beam for optimized optimal impact.

In general, this multiplexing scheme will yield a complex valued transmission $T^{\mathrm{tot}}(\mathbf{r}) = A^{\mathrm{tot}}(\mathbf{r}) \times \exp\left[\imath\Phi^{\mathrm{tot}}(\mathbf{r})\right]$ with amplitude and phase information. Different approaches exist to realize such a transmission as phase-only hologram, see, e.g., Arrizón *et al.* [40]. However, a particularly efficient and simple solution represents $A^{\mathrm{tot}}(\mathbf{r}) = \mathbb{1}$, thus setting the amplitude modulation to unity and directly use $T^{\mathrm{tot}}(\mathbf{r}) = \exp\left[\imath\Phi^{\mathrm{tot}}(\mathbf{r})\right]$ as phase-only transmission. This approach will yield optical powers in unwanted diffraction orders, but, nonetheless, will be significantly more efficient than aforementioned phase-coding techniques. However, it has negative impact on the uniformity of individual spots. To restore equal power distribution a set of constant phase offsets $\{\phi_j\}$ in the grating representation of Eq. (1) can be found by an iterative optimization routine. Here, the optical field in the working volume and the optical power of the $j_{\max}$ spots have to be simulated for each iteration [41]. This iterative Fourier-transform algorithm [42] is expanded to all three spatial dimensions (3D–IFTA) and yields the phase offsets $\{\phi_j\}$ until a desired uniformity or weighting is reached. The deduced set of $\{\phi_j\}$, finally, completely determines the total phase-only transmission T^{tot} for each spot placed in the working volume by $\{\mathbf{K}_j, f_j\}$. Please note that the spot distribution can be designed with an arbitrary weighting as required.

The spatial resolution of today's SLMs already allows to split the raw beam into several hundred volume-split focus copies. Depending on the target focus distribution and applied spatial frequencies, efficiencies are achieved between 70 % and 90 %. The number of spots can be further increased when using stationary diffractive optical elements (DOEs) to realize T^{tot}. Typically, after having applied soft quantization [43] on available phase levels the diffraction efficiency reaches values comparable to those when using SLMs. However, the amount of unmodulated light is significantly reduced when DOEs are employed. Two selected examples of phase modulations Φ^{tot} defining T^{tot} are depicted in Fig. 2. In both cases phase quantization on 8 levels were applied to Φ^{tot} optimized for the laser lithographic realization in fused silica.

The corresponding focus distributions of these two phase holograms can be seen in Figs. 3 and 4 where tens-of-spots are distributed along a spiral-like trajectory and a cone surface, respectively. After

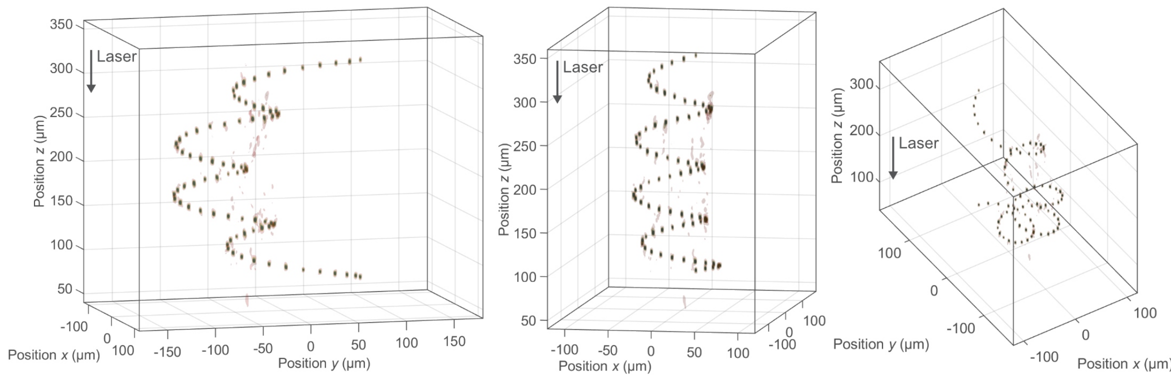

Fig. 3: Measured intensity $I\left(x,y,z\right)$ in an isosurface representation [32] of a 3D-focus distribution consisting of 70 spots and following a screw-like trajectory $\mathbf{K}\left(t\right)=\left(x\left(t\right),y\left(t\right),z\left(t\right)\right)=\left(a_1\sin\left(a_2t\right),a_1\cos\left(a_2t\right)+a_3t^2,a_4t+a5\right)$, for $0\leq t<1\in\mathbb{R}$, with $\left(a_1,a_2,\ldots,a_5\right)=$ const. $\in\mathbb{R}$. Micrometer-scaled laser beam characterization was achieved by microsopy of the focal volume using a reversed focusing setup similar to the one shown in Ref. [45]. Every subfigure depicts the same focus distribution from different perspectives.

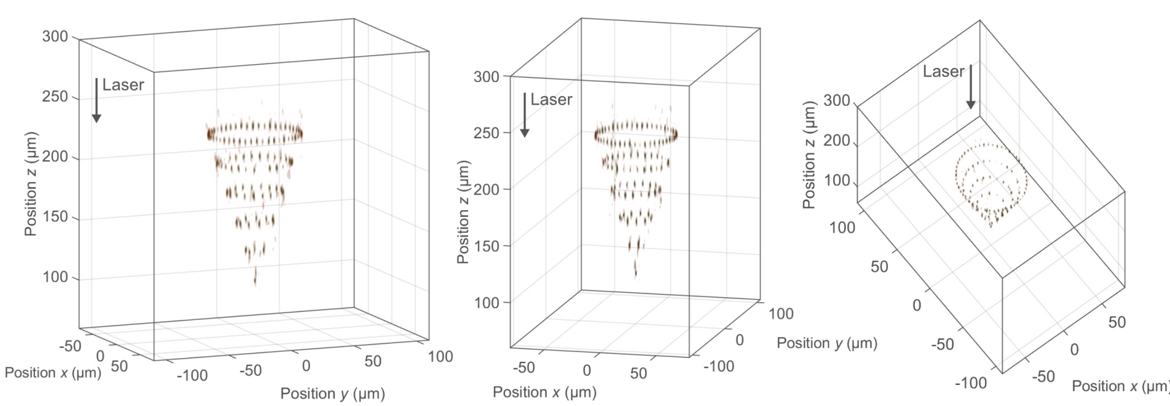

Fig. 4: Measured intensity $I\left(x,y,z\right)$ in an isosurface representation [32] of a 3D-focus distribution consisting of 120 focus copies arranged along a cone surfaces. Micrometer-scaled laser beam characterization was achieved by microsopy of the focal volume using a reversed focusing setup similar to the one shown in Ref. [45]. The peak intensity per spot deviates by less than $5\,\%$ from the mean value confirming a successful optimization routine. Every subfigure depicts the same focus distribution from different perspectives.

having focused the spot distribution in a sub-millimeter-scaled working volume using an NA-0.4-microscope objective and a $2f$-like configuration, the same optical concept was used in a reversed way to perform the laser beam characterization with an NA of 0.4 [45]. The measured data confirms a successful volume-beam splitting concept with highest spot densities and uniformities along the accelerating trajectory and the cone surface, respectively.

As can be seen from the two measurements (Figs. 3 and 4) as well as from the simulation depicted in Fig. 1 (c), holographic beam splitting produces undesired side orders that can also reach significant relative intensities of $> 10\,\%$. The actual value of the unwanted local intensity maxima depends on the spot density and arrangement and can be suppressed by the iterative design algorithm. Please note that the spot density cannot be chosen arbitrarily high, as interference of the multiplexed signals will cause beating effects reducing uniformity. However, as will be demonstrated in Sec. 4, neither discrete sampling nor unwanted side orders have a negative impact on the machining result. The simultaneous introduction of the modifications ensures their interconnection and a continuous etch access, although the desired trajectory does not exhibit continuous high intensities. Peak intensities in unwanted diffraction orders are below the substrate's nonlinear absorption threshold and do not lead to volume modifications. A technique for further increasing spot density while suppressing interference effects is proposed in Ref. [46]. Here, polarization beam splitting is applied providing focus copies with alternating polarization states.

3 Large-working-volume focusing units

In the foregoing section, we discussed the basics of simultaneously generating a large number of spots in a given working volume along a desired curved trajectory or surface. To handle the high numerical complexity of wave-optical hologram design [14, 36], we make use of ideal optical elements (thin-element approximation) as well as the angular spectrum method and far-field operators [38]. Now, the question arises whether a *real* focusing unit is in principle capable of delivering diffraction-limited focal spots in the required working volume. Ideally, the uniformity of the spot distribution, cf. Fig. 3, is not affected by the real objective and the single spots show radial symmetric profiles without preferential direction. In addition, an industrially suitable machining is aimed where the focusing unit efficiently provides the focus shape with a sufficient working distance and is able to resist ultrashort laser pulses in the millijoule class [14, 47]. In the following, we will focus on micromachining of display glasses of $d \approx 0.5\,\mathrm{mm}$ thickness, cf. Sec. 4, and, thus require a working volume of $V \approx d^3$ (please note, that our beam splitter concept is not restricted to the micrometer regime and can be scaled with the focal length of the focusing unit). Considering cleaving of display glasses with non-diffracting beams (straight glass edges) [23, 48, 49], we aim for focus dimensions in the range of $(1 \ldots 5)\ \mu\mathrm{m}$. The focusing device should therefore feature a numerical aperture of $\mathrm{NA} \gtrsim 0.2$ and an effective focal length of $f_{\mathrm{eff}} \lesssim 20\,\mathrm{mm}$, for further specifications see overview provided in Ref. [47].

As mentioned above, the demands on the imaging performance of the microscope lenses are high as aberrations within the comparatively large working volume should be negligibly small. In practical applications, however, a large axial and lateral working volume lead to an inherent physical limitation and conflicts especially high numerical apertures. An absence of lateral aberrations requires the system to satisfy the Abbe sine condition [50]. Hence residual spherical aberrations will occur along the axial dimension. On the other hand, the absence of axial aberrations requires the Herschel condition to be satisfied resulting in remaining lateral aberrations mainly composed by coma [50]. In detail, here, the rotational symmetry of the individual focal points is essential for a controlled laser modification process as non-radial symmetric spots can generate cracks whose orientation may not be aligned with the processing direction. Please note that if alignment of the preferred direction induced by non-axisymmetric focal points and the processing direction is ensured the glass separation step can be facilitated significantly [23, 51]. However, laser modifications with uncontrolled crack orientation usually result in poor edge quality. Therefore, the microscope lenses have been designed to satisfy the sine condition and weak spherical aberrations remain along the axial range [47].

To demonstrate the need for a multi-lens focusing objective when processing large volumes with NAs above 0.2, ray- and wave-optical simulations were performed shown in the scenario of Fig. 5. Here, the performance of a conventional (single lens) asphere (top) and a microscope objective (six lenses and cover glass, bottom) can be directly compared. The simple optical setup comprises mainly the beam splitter and the focusing unit in a $2f$-like arrangement [14, 16], represented by black boxes, see left hand side. As mentioned, for the tailored-edge cleaving of glasses relevant for display industry, a working volume is aimed with $V \approx (500\,\mu\mathrm{m})^3$. For this reason, three focusing scenarios were investigated, where three spots are distributed at following coordinates volume: $(y = -250\,\mu\mathrm{m}, z = -250\,\mu\mathrm{m})$, $(y = 0\,, z = 0\,)$, and $(y = 250\,\mu\mathrm{m}, z = 250\,\mu\mathrm{m})$. Here, the focus at $(y = 0\,, z = 0\,)$ is on the geometrical focus of the focusing unit serving as reference. For the sake of simplicity, in all three cases the distribution of the spots is kept at two dimensions only and $x = 0$ is set. The ray- and wave-optical evaluation of the resulting foci confirms the need for a multi-lens microscope objective as diffraction limited spots were achieved even at the limits of the working volume, see numerical results shown on the bottom right. On the other hand, the aspherical lens shows, especially in two cases at the edges of the volume, strong aberrations consisting mainly of coma, see top right. Here, resulting peak intensities $I_{\max}$ are reduced by almost one order of magnitude [47].

Upon closer inspection, one can also see the impact of our design strategy for the objective unit satisfying the Abbe sine condition [50]. In all three cases, the intensity distributions are radially symmetric and marginally modulated on axis, see bottom right of Fig. 5—a typical behavior for slightly spherically aberrated spots. Thus, the Herschel condition is not fully satisfied in the three cases shown. However, these aberrations are negligible since the peak intensities and focal shapes are mainly responsible for useful laser modifications. Here, the loss in peak intensity is smaller than 10% when using the microscope objectives, see bottom right. The beam propagation factor M^2_{eff} for general astigmatic beams, determined virtually according to ISO11146–3 [52, 53] is at the diffraction limit in the ray-optical focus and better than 1.4 at the edges of the working volume. The qualification of a focusing unit by means of a beam propagation ratio, thus by a single parameter, is of course insufficient but highly interesting from a laser technological point of view [47].

The situation using the single lens asphere is likewise clear. Optimized for the position in the geometrical focus, see middle case depicted on the top right of Fig. 5, the two other cases show strong typical coma and astigmatism aberrations at the edges of the working volume. The spot profiles are no longer radially symmetric and show significant peak intensity losses. Thus, neither the Abbe sine, nor the Herschel condition is satisfied [54]. This is confirmed by corresponding M^2_{eff}-parameters that amount to approximately 10. Therefore, simultaneous processing of a large working volume, $V \gtrsim (500\,\mu\mathrm{m})^3$, with multiple spots of $\mathrm{NA} > 0.2$ and conventional focusing units is not recommended [47].

4 Single-pass tailored-edge glass cleaving

With the previous sections (Secs. 2 and 3) we have laid the hardware fundamentals for advanced volume processing of transparent materials. Using our photonic shaping tool, various processing strategies are conceivable ranging from welding [55] to data storing [56] and waveguide writing [57]. In our opinion, however, the cutting of display glass with a tailored edge represents the greatest potential from an economical point of view.

Irrespective of whether a conventional scribe and break process [58] or a laser-based approach is used for glass cutting [23], the first process result is always a substrate with a vertical edge. These manufactured smallest edge radii represent the greatest weak points of brittle-hard materials, as stresses accumulate at the 90-deg corners which lead to chippings and cracks in the event of an impact. Substrates with reduced tangential edge angles [16], as known from beveled, chamfered or C-shaped edges, will be characterized by higher mechanical stabilities [16, 17, 59].

If a glass substrate is cut to size, various further process steps are needed, such as cleaning, polishing, hardening, etc. The longer and more complex the further processing of a substrate, the more probable it is

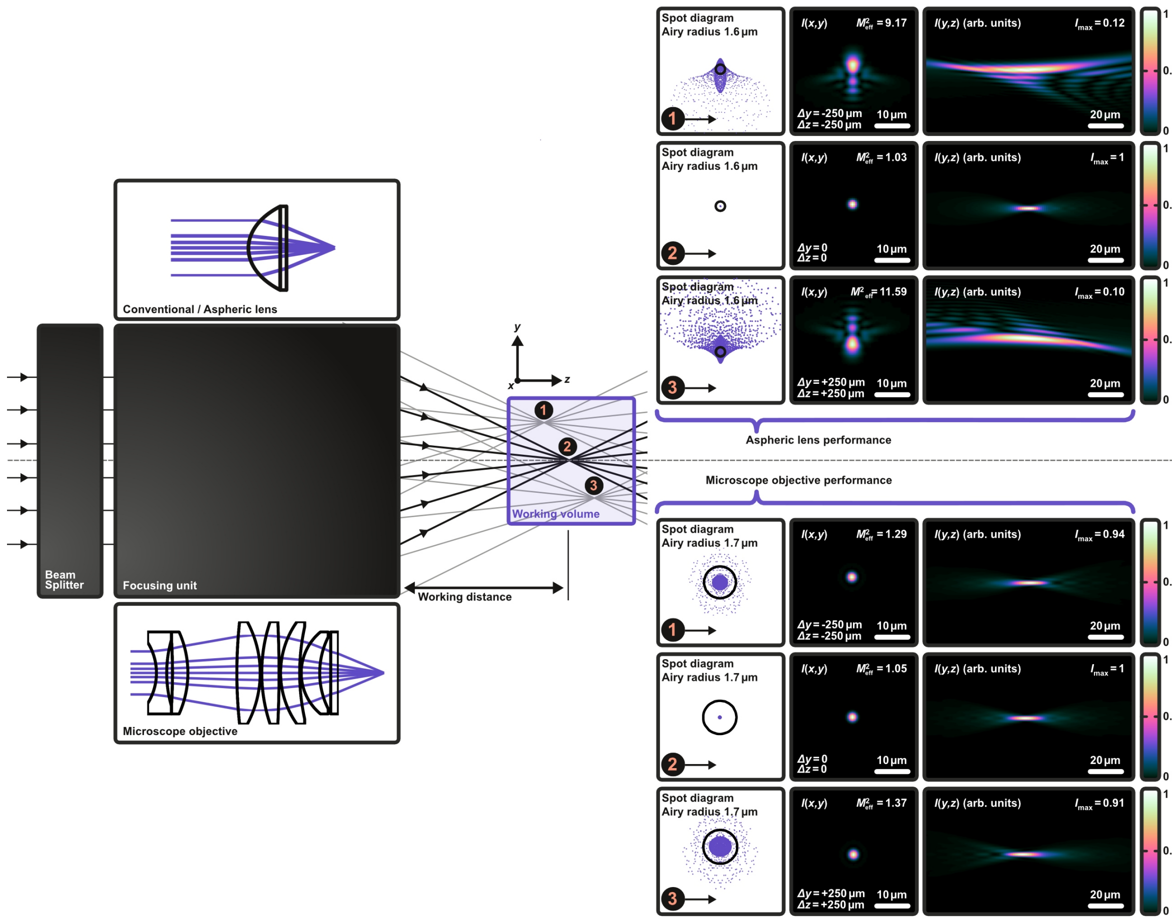

Fig. 5: Comparison of the focusing performance of a conventional single aspheric lens (top) and an adapted multi-lens microscope objective (bottom) for large volume processing with holographic 3D-beam splitters [47]. The effective focal length and the numerical aperture is set to $f_{\mathrm{eff}} = 10\,\mathrm{mm}$ and NA $= 0.45$ for both cases. The beam splitter and the focusing unit form the optical setup in a $2f$-like configuration [14, 16, 47] denoted by the black boxes (left). A working volume of $\sim (500\,\mu\mathrm{m} \times 500\,\mu\mathrm{m} \times 500\,\mu\mathrm{m})$, see purple square, is our target for the tailored-edge cleaving of display glasses. Here, three focusing situations are compared where three spots are independently distributed in the working volume: ❶ at $(y = -250\,\mu\mathrm{m}, z = -250\,\mu\mathrm{m})$, ❷ at $(y = 0\,, z = 0\,)$, and ❸ at $(y = 250\,\mu\mathrm{m}, z = 250\,\mu\mathrm{m})$, where case ❷ equals the geometrical focus of both focusing units. For simplicity, the distribution of the spots is kept at two dimensions and $x = 0$ is set for all three cases. The ray- and wave-optical evaluation of the resulting foci confirms the need for a multi-lens microscope objective as we achieve diffraction limited spots even at the limits of the working volume. The poor focusing performance of the single aspherical lens can be seen especially for the two large focus shifts, cases ❶ and ❸. Here, the transverse intensity profile $I\,(x, y)$ is no longer radial symmetric and the corresponding propagation $I\,(y, z)$ shows an accelerating behavior mainly due to coma aberrations. Resulting peak intensities I_{max} are reduced by one order of magnitude, see I_{max}-parameter in the respective $I\,(y, z)$-simulation on the right hand side [47].

that defects will occur. Here, too, a shaped glass edge will be very effective in protecting the substrate from cracks. Chamfering is therefore highly desirable right from the first process steps. Laser-based processing becomes particularly attractive when cutting and chamfering can be performed in a single processing step. [16].

Our photonic shaping tool is designed to take the shape of a desired edge geometry. Thus, several transmission functions T^{tot}, cf. Eq. (3), haven been iteratively determined and displayed by the SLM acting as flexible holographic 3D-beam splitter to fabricate glass substrates with, for example, chamfered and C-shaped egdes. Ultrashort laser pulses emerged from a TruMicro Series 2000 laser [60] are illuminating this central beam splitting element in a $2f$-like configuration, cf. Fig. 5. During machining, laser parameters were set to generate type-III-like modifications [61] inside the glass substrate. Here, a pulse energy of $\lesssim 150\,\mu\mathrm{J}$ was equally distributed to picosecond pulse trains [62, 63]. The feed rates were selected to produce a modification pitch of $\sim 5\,\mu\mathrm{m}$. Results of the first step of our glass chamfering approach, the laser modification step using volume-split spots, can be inspected in Fig. 6. Shown here is a microscope image taken perpendicularly from the edge of an unhardened $550\,\mu\mathrm{m}$-thick Corning Gorilla® glass substrate. While focusing was achieved parallel to the z-axis, see the coordinate system, the workpiece was positioned in y-direction with respect to the optical head.

The holographically split Gaussian foci cause modifications, which are partially separated and partially overlapping and which clearly follow the desired chamfer contour. All modifications are aligned parallel to the optical axis and project into the good part of our workpiece, depending on the respective position on the trajectory. This behavior is typical for type-III-regime modifications generated by Gaussian foci [64, 65]. Here, however, due to the simultaneous introduction of a large number of damages, an interaction among the modifications also takes place. Please note that, as can be seen from the microscope image, defects are at least partially connected by cracks. This points out the importance of not considering the modifications generated by the focus copies in isolation from each other, but rather to treat the entirety of the foci as *one* focus distribution. Crucial for the presented method is the simultaneity when introducing the material modifications. Only the simultaneous impact of many focal points on the material produces connected modifications without shielding effects, which in turn enable the substrate separation in the first place [16].

Please note that the laser parameters given in this study represent useful values and may form the basis for future investigations. However, we do not claim to have found the optimal parameters. Depending on the substrate geometry and material, adapted laser parameters have to be found. Furthermore, it will strongly depend on which separation process (e.g. chemical versus thermal) is actually aimed at. Especially for thermal separation with CO_2-laser radiation, which is highly relevant from an industrial point of view, the required laser parameters will be completely different and further parameter studies are necessary [16].

Various strategies are known for the second processing step, such as the application of mechanical loads [23] or the induction of thermal stresses from CO_2-laser radiation [58]. It is also well understood that different types of laser-induced modifications, for example type II modifications in fused silica [66, 67], can feature much larger etch rates than the untreated glass volume ($> 1000:1$). This selective laser-induced etching concept enables rapid fabrication of 3D-glass structures of arbitrary shapes with structural features down to the $10\,\mu\mathrm{m}$-scale [66, 67].

Our selective laser etching strategy is based on the application 30 wt.-% KOH solution to the laser-modified substrate in an ultrasonic bath at $80\,^{\circ}\mathrm{C}$ [45, 68]. After an etching time of $< 60\,\mathrm{min}$ separation is achieved, made possible by the fact that the laser-induced modifications are at least partially connected by cracks, cf. Fig. 6 [16]. Processing results are shown in Fig. 7 with scanning electron micrographs demonstrating a successful tailored-edge processing. It is straightforward to see that the edges have taken the shape of the respective focus distribution shown additionally in the top row of Fig. 7. Achieved edge surface roughness parameters were determined to $S_a < 2\,\mu\mathrm{m}$ [16] which are, thus, insignificantly higher than when cutting straight face edges with ultrafast non-diffracting beams [23]. For evidence of improved mechanical properties, we refer to the investigation in Ref. [16], in which edge stability of C-shaped display glasses was tested by means of four-point bending tests.

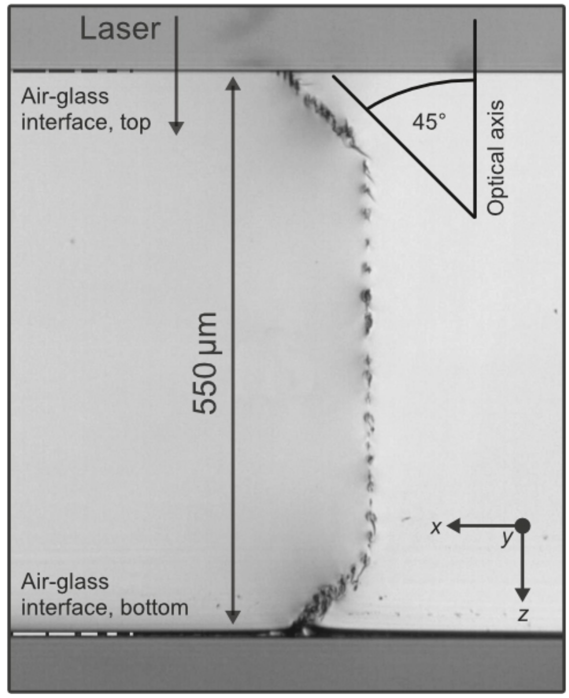

Fig. 6: Microscope image of the edge of an unhardened $550\ \mu\mathrm{m}$-thick Corning Gorilla® glass substrate with laser-induced modifications following a chamfered trajectory. Spatially separated type-III-regime modifications [61] caused by the split Gaussian foci are apparent which are at least partially connected by cracks [16, 23]. Tangential angles to the modified contour induced within a single pass are reduced down to $\alpha \lesssim 45°$. Processing was achieved parallel to the y-axis, see coordinate system. Employed pulse energy in burst mode was about $100\ \mu\mathrm{J}$—barely enough to generate visible volume modifications at all spots. Please note that not all modifications can be clearly identified by naked eye or with a light microscope, respectively.

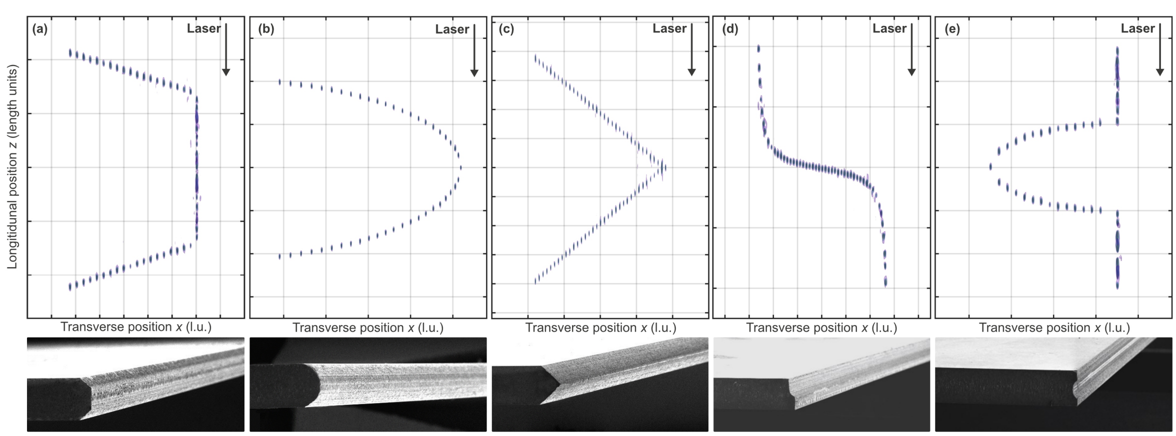

Fig. 7: Examples for 2D-focus distributions (top, the third spatial dimension is not used here) and corresponding processing results in $550\ \mu\mathrm{m}$-thick Corning Gorilla glass (bottom) [47]. In each case, the z-axis corresponds to the propagation direction. Length dimensions not shown on purpose. For the sake of clarity, the spots are weighted equally. Depending on the material, edge geometry and separation strategy, an adapted weighting is reasonable and possible. The first two examples of a chamfered (a) and a C-shaped edge (b) follow the argumentation of edge protecting due to a reduced tangential angle to the surface [16] which read as 45-deg in (a) and less than 30-deg in (b). The last three cases of an apex shape with 90-deg apex angle (c), (smoothed) step profile (d), and inverse half-circle shape (e) may be beneficial for auto-centering or flush-closing tasks [47].

5 Conclusion

We have introduced photonic tools in which the focus distribution generated from a processing optics take the shape of the workpiece to be processed. Here the two main enabler of the optical head, the holographic 3D-beam splitter and the large-working volume focusing unit were presented and corresponding design strategies were discussed. The possible shapes that this sophisticated laser tool can exhibit are enormously diverse and exceed those from well-known techniques where accelerating beams are used, especially with respect to possible radii of curvature. Applying this approach to ultrashort laser pulses allows to deposit energy at arbitrary locations in a glass volume. At the resulting material modifications the substrate can be separated, for example, by chemical means. The uniqueness of our laser optical concept is demonstrated by presenting selected processing highlights useful for edge-protecting applications. Here, cutting and edge-chamfering was performed within a single pass and with the potential for m/s feed rates.

References

[1] G. A. Siviloglou and D. N. Christodoulides, "Accelerating finite energy Airy beams," *Optics letters* **32**(8), pp. 979–981, 2007.

[2] G. Siviloglou, J. Broky, A. Dogariu, and D. Christodoulides, "Observation of accelerating Airy beams," *Physical Review Letters* **99**(21), p. 213901, 2007.

[3] N. K. Efremidis, Z. Chen, M. Segev, and D. N. Christodoulides, "Airy beams and accelerating waves: an overview of recent advances," *Optica* **6**(5), pp. 686–701, 2019.

[4] A. Mathis, F. Courvoisier, L. Froehly, L. Furfaro, M. Jacquot, P.-A. Lacourt, and J. M. Dudley, "Micromachining along a curve: Femtosecond laser micromachining of curved profiles in diamond and silicon using accelerating beams," *Applied Physics Letters* **101**(7), p. 071110, 2012.

[5] D. McGloin and K. Dholakia, "Bessel beams: diffraction in a new light," *Contemporary physics* **46**(1), pp. 15–28, 2005.

[6] J. Baumgartl, M. Mazilu, and K. Dholakia, "Optically mediated particle clearing using Airy wavepackets," *Nature photonics* **2**(11), pp. 675–678, 2008.

[7] M. Woerdemann, *Structured Light Fields: Applications in Optical Trapping, Manipulation, and Organisation*, Springer Science & Business Media, 2012.

[8] L. Froehly, F. Courvoisier, A. Mathis, M. Jacquot, L. Furfaro, R. Giust, P. Lacourt, and J. Dudley, "Arbitrary accelerating micron-scale caustic beams in two and three dimensions," *Optics express* **19**(17), pp. 16455–16465, 2011.

[9] D. M. Cottrell, J. A. Davis, and T. M. Hazard, "Direct generation of accelerating Airy beams using a 3/2 phase-only pattern," *Optics letters* **34**(17), pp. 2634–2636, 2009.

[10] P. Zhang, Y. Hu, D. Cannan, A. Salandrino, T. Li, R. Morandotti, X. Zhang, and Z. Chen, "Generation of linear and nonlinear nonparaxial accelerating beams," *Optics letters* **37**(14), pp. 2820–2822, 2012.

[11] M. Jenne, D. Flamm, T. Ouaj, J. Hellstern, J. Kleiner, D. Grossmann, M. Koschig, M. Kaiser, M. Kumkar, and S. Nolte, "High-quality tailored-edge cleaving using aberration-corrected Bessel-like beams," *Optics Letters* **43**(13), pp. 3164–3167, 2018.

[12] D. Sohr, J. U. Thomas, and S. Skupin, "Shaping convex edges in borosilicate glass by single pass perforation with an Airy beam," *Optics Letters* **46**(10), pp. 2529–2532, 2021.

[13] C. Ungaro and A. Liu, "Single-pass cutting of glass with a curved edge using ultrafast curving bessel beams and oblong Airy beams," *Optics & Laser Technology* **144**, p. 107398, 2021.

[14] D. Flamm, D. G. Grossmann, M. Sailer, M. Kaiser, F. Zimmermann, K. Chen, M. Jenne, J. Kleiner, J. Hellstern, C. Tillkorn, *et al.*, "Structured light for ultrafast laser micro-and nanoprocessing," *Optical Engineering* **60**(2), p. 025105, 2021.

[15] D. A. Green, "A colour scheme for the display of astronomical intensity images," *arXiv preprint arXiv:1108.5083* , 2011.

[16] D. Flamm, M. Kaiser, M. Feil, M. Kahmann, M. Lang, J. Kleiner, and T. Hesse, "Protecting the edge: Ultrafast laser modified C-shaped glass edges," *Journal of Laser Applications* **34**(1), p. 012014, 2022.

[17] P. Bukieda, K. Lohr, J. Meiberg, and B. Weller, "Study on the optical quality and strength of glass edges after the grinding and polishing process," *Glass Structures & Engineering* **5**, pp. 411–428, 2020.

[18] D. H. Sutter, T. Dietz, D. Bauer, R. Scelle, A. Budnicki, A. Killi, M. Jenne, J. Kleiner, D. Flamm, M. Sailer, *et al.*, "High power and high energy ultrafast disk lasers for industrial applications," in *CLEO: Science and Innovations*, pp. JM3E–2, Optical Society of America, 2019.

[19] T. G. Mans, M. Blecher, A. Hage, C. Paradis, M. Swantusch, J. Dolkemeyer, and C. Schnitzler, "High average power 10GW laser sources," in *Solid State Lasers XXX: Technology and Devices*, **11664**, p. 116640O, SPIE, 2021.

[20] J. Dominik, M. Scharun, M. Rampp, B. Dannecker, D. Bauer, T. Metzger, A. Killi, and T. Dekorsy, “Thin-disk multipass amplifier for kilowatt-class ultrafast lasers above 100 mJ,” in *The European Conference on Lasers and Electro-Optics*, p. ca_6_3, Optica Publishing Group, 2021.

[21] J. Dominik, J. Jaksic, K. Ertel, B. Dannecker, M. Scharun, S. Nagel, S. Klingebiel, T. Vogel, C. Saraceno, T. Metzger, *et al.*, “Thin-disk Multipass Amplifier for 100 mJ Class, Multi-kW High Intensity Lasers,” in *High Intensity Lasers and High Field Phenomena*, pp. HW4B–4, Optica Publishing Group, 2022.

[22] Hosseini, S Abbas and Herman, Peter R, “Method of material processing by laser filamentation,” Mar. 28 2016. US Patent 10,399,184.

[23] M. Jenne, D. Flamm, K. Chen, M. Schäfer, M. Kumkar, and S. Nolte, “Facilitated glass separation by asymmetric Bessel-like beams,” *Optics Express* **28**(5), pp. 6552–6564, 2020.

[24] M. Kumkar, M. Kaiser, J. Kleiner, D. Grossmann, D. Flamm, K. Bergner, and S. Nolte, “Ultrafast laser processing of transparent materials supported by in-situ diagnostics,” in *Laser Applications in Microelectronic and Optoelectronic Manufacturing (LAMOM) XXI*, **9735**, p. 97350P, International Society for Optics and Photonics, 2016.

[25] C. Tillkorn, A. Heimes, D. Flamm, S. Dorer, T. Beck, J. Hellstern, F. Marschall, and C. Lingel, “Anamorphic beam shaping for efficient laser homogenization: methods and high power applications,” in *Laser Resonators, Microresonators, and Beam Control XX*, **10518**, pp. 229–240, SPIE, 2018.

[26] D. Flamm, J. Hellstern, A. Heimes, F. Zimmermann, A. Ghazagh, J. Wohletz, F. Kimmich, J. Kleiner, and C. Tillkorn, “Multi-mj ultrafast laser machining with flexible multi-spot patterns,” in *High-Power Laser Materials Processing: Applications, Diagnostics, and Systems XI*, **11994**, pp. 146–152, SPIE, 2022.

[27] M. Kumkar, M. Kaiser, J. Kleiner, D. Flamm, D. Grossmann, K. Bergner, F. Zimmermann, and S. Nolte, “Throughput scaling by spatial beam shaping and dynamic focusing,” in *Laser Applications in Microelectronic and Optoelectronic Manufacturing (LAMOM) XXII*, **10091**, p. 100910G, International Society for Optics and Photonics, 2017.

[28] N. Streibl, “Beam shaping with optical array generators,” *Journal of Modern Optics* **36**(12), pp. 1559–1573, 1989.

[29] H. Ren, H. Lin, X. Li, and M. Gu, “Three-dimensional parallel recording with a debye diffraction-limited and aberration-free volumetric multifocal array,” *Optics letters* **39**(6), pp. 1621–1624, 2014.

[30] L. Zhu, M. Sun, M. Zhu, J. Chen, X. Gao, W. Ma, and D. Zhang, “Three-dimensional shape-controllable focal spot array created by focusing vortex beams modulated by multi-value pure-phase grating,” *Optics express* **22**(18), pp. 21354–21367, 2014.

[31] M. Gu, X. Li, and Y. Cao, “Optical storage arrays: a perspective for future big data storage,” *Light: Science & Applications* **3**(5), p. e177, 2014.

[32] A. Jesacher and M. J. Booth, “Parallel direct laser writing in three dimensions with spatially dependent aberration correction,” *Optics express* **18**(20), pp. 21090–21099, 2010.

[33] R. D. Simmonds, P. S. Salter, A. Jesacher, and M. J. Booth, “Three dimensional laser microfabrication in diamond using a dual adaptive optics system,” *Optics express* **19**(24), pp. 24122–24128, 2011.

[34] R. J. Noll, “Zernike polynomials and atmospheric turbulence,” *J. Opt. Soc. Am.* **66**, pp. 207–211, Mar 1976.

[35] V. A. Soifer and M. A. Golub, *Laser beam mode selection by computer generated holograms*, CRC Press, 1994.

[36] D. Flamm, D. G. Grossmann, M. Jenne, F. Zimmermann, J. Kleiner, M. Kaiser, J. Hellstern, C. Tillkorn, and M. Kumkar, “Beam shaping for ultrafast materials processing,” in *Laser Resonators, Microresonators, and Beam Control XXI*, **10904**, p. 109041G, International Society for Optics and Photonics, 2019.

[37] X. Wang, D. Wilson, R. Muller, P. Maker, and D. Psaltis, “Liquid-crystal blazed-grating beam deflector,” *Applied Optics* **39**(35), pp. 6545–6555, 2000.

[38] J. W. Goodman, “Introduction to Fourier optics. 3rd,” *Roberts and Company Publishers* , 2005.

[39] H. Itoh, N. Matsumoto, and T. Inoue, “Spherical aberration correction suitable for a wavefront controller,” *Optics Express* **17**(16), pp. 14367–14373, 2009.

[40] V. Arrizón, U. Ruiz, R. Carrada, and L. A. González, “Pixelated phase computer holograms for the accurate encoding of scalar complex fields,” *JOSA A* **24**(11), pp. 3500–3507, 2007.

[41] M. Leutenegger, R. Rao, R. A. Leitgeb, and T. Lasser, “Fast focus field calculations,” *Optics express* **14**(23), pp. 11277–11291, 2006.

[42] F. Wyrowski and O. Bryngdahl, “Iterative fourier-transform algorithm applied to computer holography,” *JOSA A* **5**(7), pp. 1058–1065, 1988.

[43] F. Wyrowski, “Iterative quantization of digital amplitude holograms,” *Applied optics* **28**(18), pp. 3864–3870, 1989.

[44] F. Wyrowski, H. van Esdonk, R. J. Zuidema, S. Wadmann, and G. J. Notenboom, “Use of diffractive optics in material processing,” in *Diffractive and Holographic Optics Technology*, **2152**, pp. 139–144, International Society for Optics and Photonics, 1994.

[45] H. Rave, H. Heiming, P. Szumny, M. Kaiser, J. Kleiner, and D. Flamm, “Glass tube cutting with aberration-corrected non-diffracting ultrashort laser pulses,” *Optical Engineering* **60**(6), p. 065105, 2021.

[46] Flamm, Daniel and Kumkar, Malte, “Method for the laser processing of a workpiece, processing optical unit and laser processing apparatus,” May 5 2022. US Patent App. 20220258284.

[47] M. Kaiser, H. Dounassre, M. Kahmann, J. Hellstern, J. Kleiner, C. Tillkorn, and D. Flamm, "Chamfered-edge laser cleaving of transparent materials," in *Frontiers in Ultrafast Optics: Biomedical, Scientific, and Industrial Applications XXII*, **11991**, pp. 32–41, SPIE, 2022.

[48] F. Ahmed, M. S. Lee, H. Sekita, T. Sumiyoshi, and M. Kamata, "Display glass cutting by femtosecond laser induced single shot periodic void array," *Applied Physics A* **93**(1), pp. 189–192, 2008.

[49] S. Marjanovic, A. R. Nieber, G. A. Piech, H. Schillinger, S. Tsuda, and R. S. Wagner, "Laser cutting of display glass compositions," Dec. 26 2017. US Patent 9,850,160.

[50] J. J. Braat, "Abbe sine condition and related imaging conditions in geometrical optics," in *Fifth International Topical Meeting on Education and Training in Optics*, **3190**, pp. 59–64, International Society for Optics and Photonics, 1997.

[51] M. Kumkar, J. Kleiner, D. Großmann, D. Flamm, and M. Kaiser, "System for asymmetric optical beam shaping," Jan. 5 2021. US Patent 10,882,143.

[52] ISO 11146-2:2005, "Lasers and laser-related equipment—Test methods for laser beam widths, divergence angles and beam propagation ratios—Part 2: General astigmatic beams," International Organization for Standardization, 2005.

[53] D. Flamm, C. Schulze, R. Brüning, O. A. Schmidt, T. Kaiser, S. Schröter, and M. Duparré, "Fast M2 measurement for fiber beams based on modal analysis," *Applied optics* **51**(7), pp. 987–993, 2012.

[54] J. H. Burge, C. Zhao, and M. Dubin, "Use of the Abbe sine condition to quantify alignment aberrations in optical imaging systems," in *International Optical Design Conference*, p. ITuD5, Optical Society of America, 2010.

[55] F. Zimmermann, S. Richter, S. Döring, A. Tünnermann, and S. Nolte, "Ultrastable bonding of glass with femtosecond laser bursts," *Applied Optics* **52**(6), pp. 1149–1154, 2013.

[56] J. Zhang, M. Gecevičius, M. Beresna, and P. G. Kazansky, "Seemingly unlimited lifetime data storage in nanostructured glass," *Physical review letters* **112**(3), p. 033901, 2014.

[57] S. Nolte, M. Will, J. Burghoff, and A. Tuennermann, "Femtosecond waveguide writing: a new avenue to three-dimensional integrated optics," *Applied Physics A* **77**(1), pp. 109–111, 2003.

[58] S. Nisar, L. Li, and M. Sheikh, "Laser glass cutting techniques—a review," *Journal of Laser Applications* **25**(4), p. 042010, 2013.

[59] S. Marjanovic, D. Andrew, P. Garrett, A. Piech, J. M. Quintal, H. Schillinger, S. Tsuda, R. S. Wagner, and A. N. Yeary, "Edge chamfering methods," Oct. 15 Oct. 15 2019. US Patent 10,442,719.

[60] F. Jansen, A. Budnicki, and D. Sutter, "Pulsed lasers for industrial applications: Fiber, slab and thin-disk: Ultrafast laser technology for every application," *Laser Technik Journal* **15**(2), pp. 46–49, 2018.

[61] K. Itoh, W. Watanabe, S. Nolte, and C. B. Schaffer, "Ultrafast processes for bulk modification of transparent materials," *MRS bulletin* **31**(8), pp. 620–625, 2006.

[62] P. R. Herman, R. Marjoribanks, and A. Oettl, "Burst-ultrafast laser machining method," Apr. 22 Apr. 22 2003. US Patent 6,552,301.

[63] C. Kerse, H. Kalaycıoğlu, P. Elahi, B. Çetin, D. K. Kesim, Ö. Akçaalan, S. Yavaş, M. D. Aşık, B. Öktem, H. Hoogland, *et al.*, "Ablation-cooled material removal with ultrafast bursts of pulses," *Nature* **537**(7618), pp. 84–88, 2016.

[64] K. Bergner, B. Seyfarth, K. Lammers, T. Ullsperger, S. Döring, M. Heinrich, M. Kumkar, D. Flamm, A. Tünnermann, and S. Nolte, "Spatio-temporal analysis of glass volume processing using ultrashort laser pulses," *Applied Optics* **57**(16), pp. 4618–4632, 2018.

[65] D. Grossmann, M. Reininghaus, C. Kalupka, M. Kumkar, and R. Poprawe, "Transverse pump-probe microscopy of moving breakdown, filamentation and self-organized absorption in alkali aluminosilicate glass using ultrashort pulse laser," *Optics Express* **24**(20), pp. 23221–23231, 2016.

[66] M. Hermans, J. Gottmann, and F. Riedel, "Selective, laser-induced etching of fused silica at high scan-speeds using KOH.," *Journal of Laser Micro/Nanoengineering* **9**(2), 2014.

[67] J. Gottmann, M. Hermans, N. Repiev, and J. Ortmann, "Selective laser-induced etching of 3D precision quartz glass components for microfluidic applications—up-scaling of complexity and speed," *Micromachines* **8**(4), p. 110, 2017.

[68] M. Kaiser, M. Kumkar, R. Leute, J. Schmauch, R. Priester, J. Kleiner, M. Jenne, D. Flamm, and F. Zimmermann, "Selective etching of ultrafast laser modified sapphire," in *Laser Applications in Microelectronic and Optoelectronic Manufacturing (LAMOM) XXIV*, **10905**, p. 109050F, International Society for Optics and Photonics, 2019.